Microstrain sensitivity of orbital and electronic phase separation in SrCrO3

Microstrain Sensitivity of Orbital and Electronic Phase Separation in $SrCrO_3$

Luis Ortega-San-Martin,[1] Anthony J. Williams,[1] Jennifer Rodgers,[1] J. Paul Attfield,[1,*] Gunter Heymann,[2] and Hubert Huppertz[2]

[1]*Centre for Science at Extreme Conditions and School of Chemistry, King's Buildings, University of Edinburgh, Edinburgh EH9 3JZ, United Kingdom*

[2]*Department Chemie, Ludwig-Maximilians-Universität München, 81377 München, Germany*

(Received 25 July 2007; revised manuscript received 23 October 2007; published 18 December 2007)

An orbital ordering transition and electronic phase coexistence have been discovered in $SrCrO_3$. This cubic, orbitally-degenerate perovskite transforms to a tetragonal phase with partial orbital order. The tetragonal phase is antiferromagnetic below 35–40 K, whereas the cubic phase remains paramagnetic at low temperatures. The orbital ordering temperature (35–70 K) and coexistence of the two electronic phases are very sensitive to lattice strain. X-ray measurements show a preferential conversion of the most strained regions in the cubic phase. This reveals that small fluctuations in microstrain are sufficient to drive long range separation of competing electronic phases even in undoped cubic oxides.

DOI: 10.1103/PhysRevLett.99.255701 PACS numbers: 64.75.+g, 61.50.Ks, 61.66.Fn, 75.25.+z

Transition metal oxides display a remarkable range of electronic phenomena such as superconductivity, metal-insulator transitions, and coupled charge, orbital, and spin orderings [1–3]. For example, orbital ordering of degenerate $t_{2g}{}^n$ configurations can stabilize spin-gapped states such as a singlet dimerized phase in $La_4Ru_2O_{10}$ [4] and possible Haldane chains in $Tl_2Ru_2O_7$ [5]. In addition, the coexistence of electronically distinct phases within a chemically homogenous matrix can lead to the emergence of notable physical properties, ranging from colossal magnetoresistances [6] to spin glass behavior in metal-insulator segregated perovskite manganites [7]. Electronic phase segregation of insulating phases based on different long range orbital orderings has also been reported in manganites [8] and in $SmVO_3$ [9]. $SrCrO_3$ was first reported to be a paramagnetic metallic oxide with a cubic perovskite structure 40 years ago [10]. There have been few subsequent investigations of the electronic properties as high pressure and temperature synthesis conditions are required [11]. However, a recent study concluded that $SrCrO_3$ shows anomalous electronic and magnetic properties resulting from bond-length fluctuations, but that "the lattice instabilities do not manifest themselves as a phase segregation" [12]. In this Letter, we show that an orbital ordering instability drives a cubic to tetragonal structural transition resulting in low temperature phase coexistence in $SrCrO_3$. The orbital ordering transition shows a remarkable sensitivity to random strains, and high resolution x-ray diffraction shows that the most strained regions in the cubic phase preferentially transform to the orbitally ordered structure.

Polycrystalline 10 mg samples of $SrCrO_3$ were prepared under pressures of 6, 8, and 10 GPa at 1000–1100 °C using a Walker type multianvil apparatus. The 6 and 8 GPa samples were prepared from a stoichiometric mixture of $Sr_3(CrO_4)_2$ and Cr_2O_3, and the synthesis of the 10 GPa sample was reported in a previous study of $SrCr_xRu_{1-x}O_3$ solid solutions [13]. All three samples are phase pure by x-ray powder diffraction and are oxygen stoichiometric within errors of 1–2% in the refined oxygen site occupancies when fitting the x-ray and neutron data below.

Initial study of the 10 GPa $SrCrO_3$ sample [13] revealed a magnetization peak at 40 K (Fig. 1), and differences between neutron diffraction profiles at 10 and 100 K appeared to signify a structural distortion. To clarify the ground state properties of $SrCrO_3$, we have recorded highly resolved synchrotron powder x-ray diffraction patterns [14]. At low temperatures, additional peaks (Fig. 2) appear around the sharp maxima expected for cubic $SrCrO_3$ ($a_C \approx 3.811$ Å). The peaks are indexed on a tetragonally-compressed cell (space group $P4/mmm$, $a_T \approx 3.822$, $c_T \approx 3.792$ Å), showing that a previously unreported tetragonal phase of $SrCrO_3$ coexists with the cubic form. No further superstructure arising from an octahedral tilting instability is observed.

Cubic $SrCrO_3$ has an orbital liquid state resulting from the triply degenerate $(d_{xy}, d_{xz}, d_{yz})^2$ configuration for Cr^{4+}, as the CrO_6 octahedra are regular with six Cr-O distances of 1.906 Å at 10 K. The Cr-O distances of 4×1.911 Å and 2×1.896 Å at 10 K in the tetragonal phase of $SrCrO_3$ do not correspond with a full Jahn-Teller splitting for Cr^{4+} but do reveal a partial orbital ordering, $d_{xy}{}^1(d_{xz}, d_{yz})^1$ in which one electron is localized. This partial orbital order is corroborated by the observation of two very weak magnetic peaks in the difference between neutron diffraction profiles at 10 and 100 K [Fig. 2(c) inset). These peaks index on an antiferromagnetic (1/2 1/2 0) superstructure of the tetragonal $SrCrO_3$ phase and are fitted by the spin ordering model shown in Fig. 1. The antiferromagnetic superexchange coupling in the xy plane and the ferromagnetic coupling along z are consistent with the localization of $d_{xy}{}^1$ orbital states in the tetragonal phase of $SrCrO_3$. No magnetic peaks from the cubic form are observed.

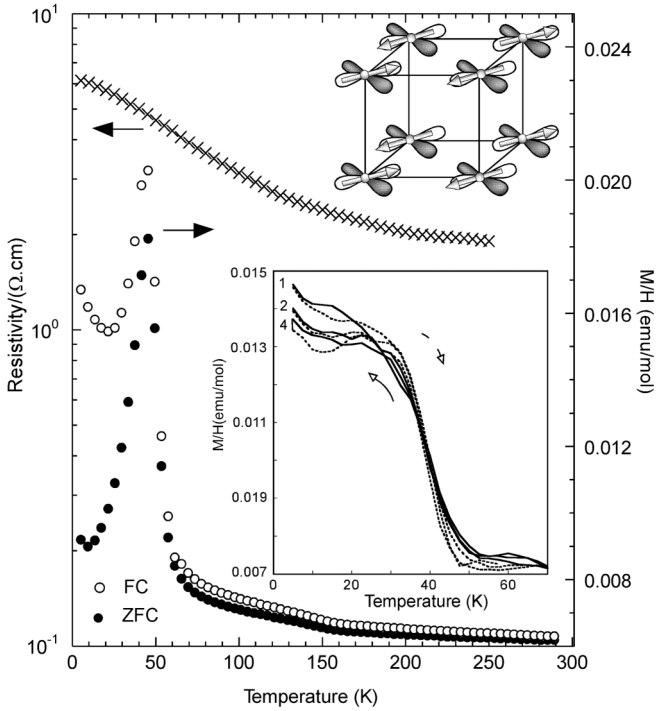

FIG. 1. Electrical resistivity and magnetization results for $SrCrO_3$. SQUID magnetization measurements in a 500 Oe field and four probe resistance measurements on a sintered bar were made using commercial instruments. The main plot shows resistivity and zero field cooled (ZFC) and field cooled (FC) magnetization/field data for the 10 GPa sample 13. The divergence between ZFC and FC magnetizations is likely to reflect the cooperative freezing scenario reported in phase separated manganites [7]. The lower inset shows the effect of cycling the 8 GPa sample between 5 and 70 K. Warming/cooling data for cycles 1, 2, and 4 are shown as broken/continuous lines. The decrease in low temperature magnetization on cycling evidences a reduction in the proportion of the tetragonal phase. The upper inset shows the $d_{xy}{}^1$ orbital order and antiferromagnetic spin order in the tetragonal phase of $SrCrO_3$.

A surprising variability in the onset temperature for orbital ordering (T_{OO}) and the degree of transformation is observed for the three $SrCrO_3$ samples, as shown in Fig. 3 and Table I. These vary from a complete cubic to tetragonal phase transformation between 70 and 20 K in the 8 GPa sample, to a ~50% conversion below $T_{OO} = 35$ K for the 10 GPa sample. The sharp magnetization change at 35–40 K for all samples coincides with the steepest growth of the tetragonal phase, suggesting that the spin order further stabilizes the orbitally ordered phase. The spin ordering temperature of 35–40 K appears to be the same in all samples although T_{OO} varies from 35 to 70 K. It is unclear at present whether spin order imposes a lower limit of 35 K on T_{OO}, or whether the transition can be driven to lower temperatures enhancing quantum orbital fluctuations. The cubic-tetragonal transition does not result in a resistive discontinuity. Our sintered $SrCrO_3$ ceramics, like those reported elsewhere [11,12], tend towards a finite resistance at low temperatures indicating itinerant electron behavior,

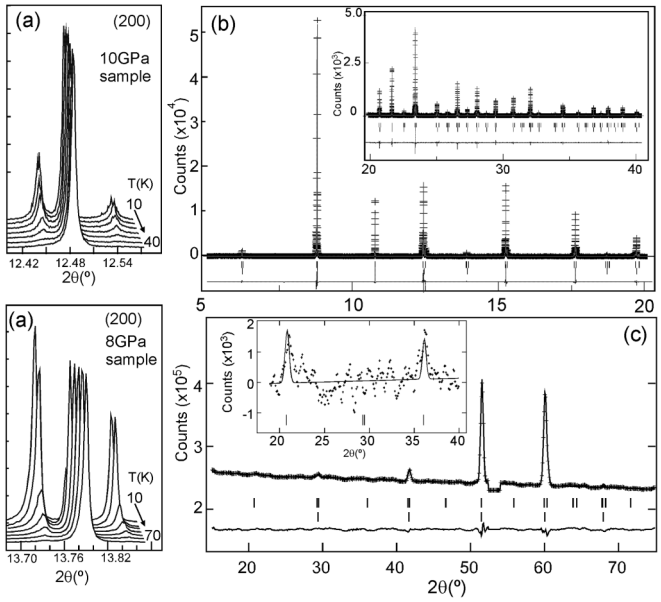

FIG. 2. Powder diffraction profiles for $SrCrO_3$; (a) The temperature evolutions of the cubic (200) synchrotron x-ray diffraction peak for the 8 and 10 GPa samples, showing the growth of additional reflections from the tetragonal phase at low temperatures. (b) Fit to the 10 K synchrotron x-ray diffraction profile of the 10 GPa sample with cubic/tetragonal reflections indicated by lower/upper tick marks. (c) Two phase fit to the 10 K neutron diffraction profile of the 10 GPa sample showing the magnetic superstructure positions. The inset shows the fit of the antiferromagnetic model in Fig. 1 to the intensity difference between 10 and 100 K neutron data. Neutron data were collected on instrument D20 at ILL, Grenoble with wavelength $\lambda = 1.8889$ Å.

but the high resistivities ($\sim 10^1$–10^2 Ω cm) which decrease on warming may be dominated by grain boundary contributions. Further work on crystals or epitaxial films will be needed to clarify the electronic transport properties of the two phases of $SrCrO_3$.

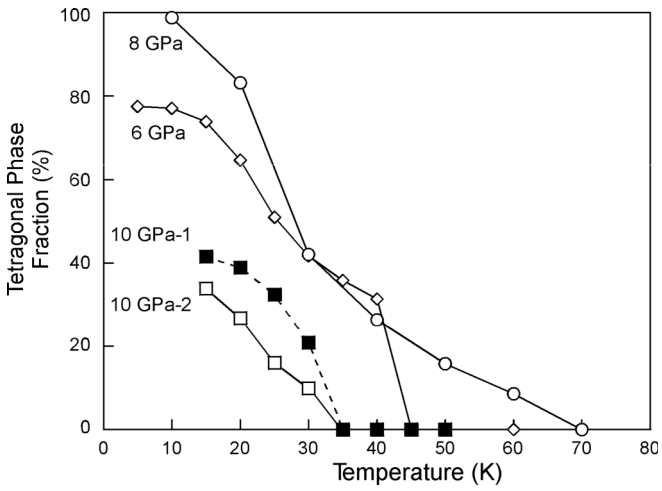

FIG. 3. Temperature variation of the tetragonal phase fraction (p_T) in samples of $SrCrO_3$ prepared at 6, 8, and 10 GPa. Data for the latter are shown while warming during cycles 1 and 2.

TABLE I. Comparison of phase separation characteristics for samples of $SrCrO_3$ prepared at 6, 8, and 10 GPa. The orbital ordering transition temperature, the lattice parameter, and microstrain for the cubic phase at 250 K, and the microstrains and tetragonal phase fraction phase at 10 K are shown. The 250 K lattice parameters were determined using the same synchrotron x-ray wavelength of 0.39832 Å and so are directly comparable.

Sample P (GPa)	6	8	10
T_{oo}(K)	45	70	35
p_T(10 K)(%)	77.1(1)	98.8(1)	36.5(2)
a_C(250 K)(Å)	3.81765(1)	3.81772(1)	3.81742(1)
s_C(250 K)(%)	0.169(1)	0.056(7)	0.143(1)
s_C(10 K)(%)	0.072(2)	0.032(2)	0.107(1)
s_T(10 K)(%)	0.212(2)	0.053(1)	0.167(2)

The orbital ordering temperatures and degrees of transformation correlate with minor variations in the cubic lattice parameter for the three $SrCrO_3$ samples, as shown in Table I. The change of T_{OO} by a factor of 2 while a_C changes by only 3×10^{-4} Å reveals an unprecedented sensitivity of the electronic transition to lattice effects, showing that the energy difference between the two electronic ground states is very small. In such situations, the lattice influence can be significant. The degree and length scale of electronic phase segregation in perovskite manganites depends upon the coupling of the macrostrains, resulting from the small differences between the lattice parameters of distinct electronic phases, to local microstrains arising from lattice defects [9]. However, it is difficult to measure accurate microstrains from diffraction peak broadenings for the individual phases in segregated manganites or vanadates because the high temperature phases have subtle superstructures due to octahedral tilting instabilities, and further lattice distortions (e.g., from orthorhombic to monoclinic symmetry at the charge ordering transition in manganites) lead to peak envelopes that have both macro and microstrain contributions [15]. However, the two phases of $SrCrO_3$ have high symmetries, and the strongly discontinuous nature of the transition [evidenced by the lattice parameters and volume variations in Fig. 4(a)] minimizes peak overlap enabling the strain broadenings and lattice parameters to be measured independently for the two phases [14]. These show the same thermal variations for all three $SrCrO_3$ samples (see Fig. 4).

The d_{xy}^1 orbital order in the tetragonal phase expands the a_T lattice parameter and contracts c_T, relative to the cubic a_C, leading to large macrostrains [e.g., the tetragonal macrostrain is $e_T = 3(a_T - c_T)/(2a_T + c_T) \approx 0.8\%$]. The tetragonal phase nucleates as highly-strained domains, which grow on cooling enabling the strains to relax, as evidenced by the rapid decreases in the tetragonal microstrain s_T, which is an order of magnitude larger than that in the parent cubic phase, s_C, and in the tetragonal lattice parameters and volume (Fig. 4). In a conventional martensitic description, the growing tetragonal regions should induce an increasing accommodation strain contribution to s_C in the surrounding matrix of the cubic phase, which may ultimately prevent further growth, leading to a mixed phase material. However, this is not seen in the s_C values which fall slightly on cooling from 250 K to T_{OO} but then *decrease* significantly below the orbital ordering transition in all three samples of $SrCrO_3$ [Fig. 4(b)]. This demonstrates that the dominant effect is the selective growth of the tetragonal phase at the most strained regions in cubic $SrCrO_3$, so that the average microstrain for the cubic phase decreases as the proportion falls on cooling. This may be a general phenomenon in phase separating oxides although it is not easily measured in other materials. Our interpretation is supported by the variations of the weighted total microstrain for the two phases, s_{Total}, which shows a maximum just below T_{OO} as the tetragonal phase nucleates, but declines towards a low temperature value similar to that of the parent cubic phase above the transition. Thus, the microstrains in the bulk sample are almost unchanged by the transformation to the tetragonal phase although they evidently have a strong influence on the local thermody-

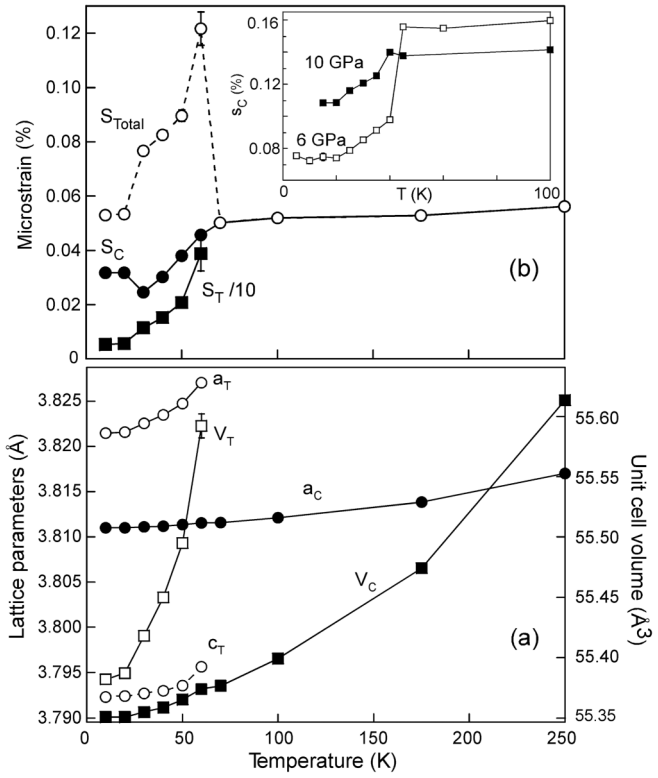

FIG. 4. Thermal evolutions of the cubic and tetragonal phases ("C" and "T" subscripts) of the 8 GPa sample of $SrCrO_3$, from fits to synchrotron x-ray diffraction profiles. (a) Lattice parameters a and c and cell volumes V. The apparently large thermal expansion of the tetragonal phase evidences large strains in the residual domains approaching the transition. (b) Microstrains for the cubic (s_C) and tetragonal (shown as $s_T/10$) phases are plotted together with the total microstrain ($s_{Total} = [p_T {s_T}^2 + (1 - p_T){s_C}^2]^{1/2}$). Inset shows s_C for the 6 and 10 GPa samples.

namics of the transition. The preferential transformation of the most strained regions in $SrCrO_3$ is supported by observations that some strain annealing can occur through thermal cycling. Repeated magnetic cycling of the 8 GPa sample (see lower inset of Fig. 1) and measurement of phase fractions in the 10 GPa sample during a second warming cycle (Fig. 3) both show a decrease in the tetragonal phase fraction p_T.

Comparing data for the three $SrCrO_3$ samples in Table I shows no correlation of the phase transformation with the synthesis pressure. The 8 GPa sample shows the highest T_{OO} and the most complete conversion and yet has the smallest microstrains in the high and low temperature phases. The apparent paradox that high microstrain suppresses the orbital ordering transition while also providing the favorable nucleation sites shows that the spatial variations of the strain field which control growth are very important. Although regions of high strain are required to nucleate the tetragonal phase, large local variations in strain disfavor growth of the tetragonal phase nuclei so that a slowly-varying strain field is likely to be more effective in promoting the transformation than a peaky one. The ability of structural inhomogeneities to nucleate and direct long range electronic phase coexistence in manganites has recently been described using a free-energy landscape approach [9], which has been supported, for example, by a magnetic force microscopy study of twinned (La, Pr, Ca)MnO_3 crystals where ferromagnetic regions were observed to grow along the twin boundaries [7]. The extension of this description to materials lacking intrinsic strain fields from La/Pr/Ca, etc., cation disorder [16] or crystal twinning has been unclear. The sensitivity of the electronic phase separation in $SrCrO_3$ to the preparation and thermal cycling of the samples, and the discovered fall in the cubic microstrain below the transition, demonstrate that very small local variations in strain are sufficient to nucleate and control the degree of phase transformation. The origin of the structural inhomogeneities in $SrCrO_3$ is unknown at present; small variations in oxygen content (below our measured accuracy of 1–2%) or residual stresses from the synthesis procedure may be responsible. Low levels of such imperfections are typically present in transition metal oxides, and our results show that these are sufficient to drive long range coexistence when two competing electronic phases with strong electron-lattice coupling are present, even in an undoped cubic material like $SrCrO_3$. A future challenge will be to control and pattern strain fields while minimizing background microstrain to create conducting or magnetic nanostructures within such chemically homogenous but electronically bistable materials.

In conclusion, $SrCrO_3$ provides a uniquely simple example of orbital ordering and phase coexistence in an undoped cubic perovskite oxide. The cubic phase is paramagnetic and remains an orbital liquid at low temperatures whereas the competing tetragonal phase has partial orbital order and is antiferromagnetic below 35–40 K. Small sample-to-sample variations in the strain field lead to unprecedented variations by a factor of 2 in the orbital ordering transition temperature and the tetragonal phase proportion, leading to phase coexistence in the high microstrain samples.

This work has been supported by EPSRC, the Leverhulme Trust and ESF COST network No. D30/003/03. L. O. S. M. acknowledges the Gobierno Vasco/Eusko Jaurlaritza (Spain) for additional support. The authors gratefully acknowledge Drs. J. W. Bos, S. Kimber, A. Fitch, I. Margiolaki, and P. Henry and Mr. W-T. Chen for their assistance with data collection at the ESRF and ILL.

*j.p.attfield@ed.ac.uk

[1] E. Dagotto, Science **309**, 257 (2005).
[2] Y. Tokura, Rep. Prog. Phys. **69**, 797 (2006).
[3] V. B. Shenoy, D. D. Sarma, and C. N. R. Rao, Chem. Phys. Chem. **7**, 2053 (2006).
[4] P. Khalifah *et al.*, Science **297**, 2237 (2002).
[5] S. Lee *et al.*, Nat. Mater. **5**, 471 (2006).
[6] M. Uehara, S. Mori, C. H. Chen, and S.-W. Cheong, Nature (London) **399**, 560 (1999).
[7] W. Wu *et al.*, Nat. Mater. **5**, 881 (2006).
[8] J. P. Chapman *et al.*, Dalton Trans. **19**, 3026 (2004).
[9] M. H. Sage, G. R. Blake, G. J. Nieuwenhuys, and T. T. M. Palstra, Phys. Rev. Lett. **96**, 036401 (2006).
[10] B. L. Chamberland, Solid State Commun. **5**, 663 (1967).
[11] E. Castillo-Martínez and M. A. Alario-Franco, Solid State Sci. **9**, 564 (2007).
[12] J.-S. Zhou *et al.*, Phys. Rev. Lett. **96**, 046408 (2006).
[13] A. J. Williams *et al.*, Phys. Rev. B **73**, 104409 (2006).
[14] Data were collected between 10 and 250 K on instrument ID31 at the ESRF, Grenoble, from capillary samples in the angular range $3° \leq 2\theta \leq 40°$ at wavelengths of 0.39–0.46 Å. Wavelengths were calibrated using a standard Si powder (NIST SRM 640c, $a = 5.4311946(92)$ Å). Rietveld profile fits were used to obtain the lattice parameters and microstrain for each phase. The diffraction peaks were described by Lorentzian functions with full width at half maxima Γ varying as $\Gamma(\text{rad}) = [s + s_i]\tan\theta$, where s is the phase microstrain (root mean-squared variation in lattice strain) and $s_i = 0.036\%$ is the instrumental broadening contribution found by fitting peaks from the Si standard. The cubic, s_C, and tetragonal, s_T, contributions were refined independently except s_C for the 8 GPa sample at 10 K was fixed at the 20 K value because of the small cubic phase fraction. Domain size broadening, which would give a $\Gamma \sim 1/\cos\theta$ dependence, was not significant for either phase at high phase fractions, although it may contribute to s_T just below the orbital ordering transition.
[15] P. G. Radaelli *et al.*, Phys. Rev. B **63**, 172419 (2001).
[16] L. M. Rodriguez-Martinez and J. P. Attfield, Phys. Rev. B **54**, R15622 (1996).